

Cover Sheet for Supporting Information (SI)

Simulation of aromatic SOA formation using the lumping model integrated with explicit gas-phase kinetic mechanisms and aerosol-phase reactions

Authors: Yunseok Im, Myoseon Jang* and Ross Beardsley

Department of Environmental Engineering Sciences, University of Florida P.O. Box 116450,
Gainesville, FL 32611, USA

Number of Figures: 9

Number of Tables: 5

Section S1. Chamber Studies

Chamber operation The University of Florida Atmospheric PHotochemical Outdoor Reactor (UF-APHOR) dual chambers are located on the roof of Black Hall (latitude/longitude: 29.64185°/-82.347883°) at the University of Florida, Gainesville, Florida. The air volume of the two half-cylinder shaped dual chambers is 104 m³ (52 m³ + 52 m³). The walls of the chamber are made of 5mil FEP Teflon film and the surface to volume ratio of each chamber is 0.20 m⁻¹. For the sunlight characterization, sunlight spectrum and intensity were measured both inside and outside of the chamber using the spectroradiometer (Apogee, PS-300) and the ultraviolet radiometer (The Eppley Laboratory, model TUVR, wavelength 290 to 385 nm), respectively. Then the sunlight source was characterized using the chamber experiment of acetaldehyde photolysis. Also, the wall loss rate constant of ozone was measured through a separate experiment.

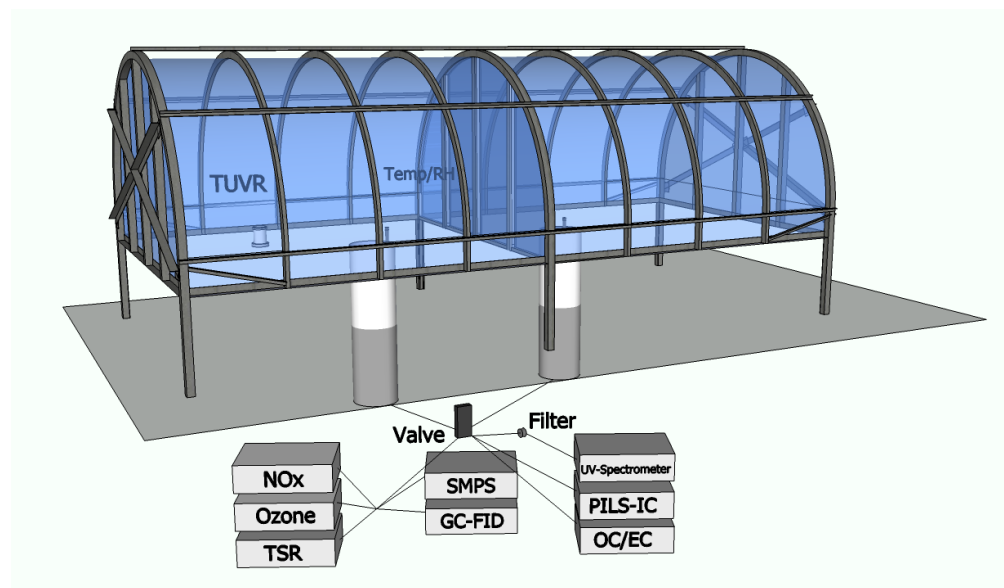


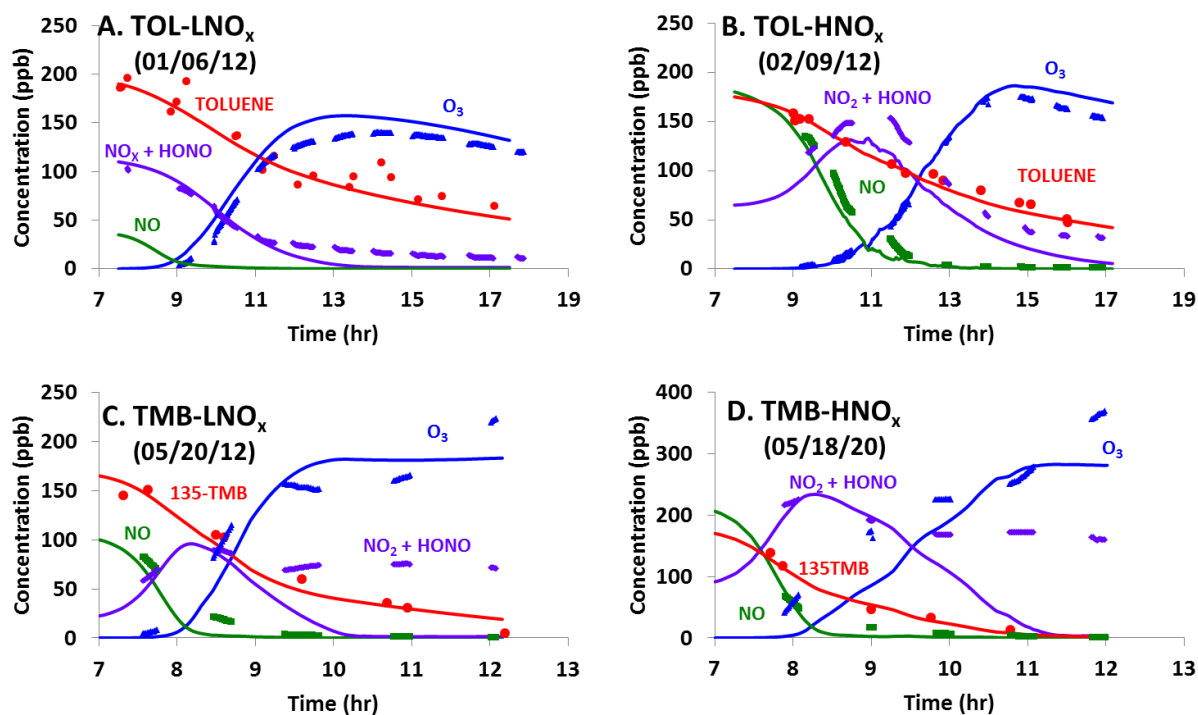
Figure S1. The University of Florida Atmospheric Photochemical Outdoor Reactor (UF-APHOR) dual chambers and experimental setup.

Experimental instruments. The gaseous and aerosol samples were directly carried to laboratory instruments from the chamber through sampling conduit that holds various sampling lines. The concentrations of AVOC and CCl₄ were monitored using a gas chromatography-flame ionization detector (HP-5890 GC-FID) with a DB5 fused silica capillary column (15 m, 0.53 mm i.d., 1.5 μm thickness, J & W Scientific INC., Cat# 1255012). The GC oven temperature was fixed at 110 °C and the carrier gas (nitrogen) flow rate was 10.0 mL min⁻¹. The concentrations of O₃ and SO₂ were monitored with a photometric ozone analyzer (Teledyne, model 400E) and a fluorescence TRS analyzer (Teledyne model 102E), respectively. Temperature and relative humidity (RH) were measured using Temp/RH sensors (Campbellscientific, CS215-L) for both chambers. The solar UV radiation was monitored by an ultraviolet radiometer (The Eppley Laboratory, model TUVR, wavelength 290 to 385 nm) installed in the East chamber. All meteorological data were recorded over the course of the experiment using the data logger system (Campbellscientific, CR800). The particle volume concentration was monitored with a scanning mobility particle sizer (SMPS, TSI, Model 3080) integrated with a condensation nuclei counter (TSI, Model 3025A and Model 3022). The SMPS sampling and sheath flow rates were 0.3 and 2 L min⁻¹, respectively. The particle wall loss rate for each particle size bin was measured as first order in a separate experiment and applied to the other chamber experiments (Keywood et al., 2004). The organic carbon (OC) content in aerosols was monitored using a semi-continuous OC/EC carbon aerosol analyzer (Sunset Laboratory, Model 4) with 40 minutes cycle (26 min sampling and 14 min analyzing). Inorganic ions in aerosols were measured using a PILS-IC (Particle into Liquid Sampler (Applikon, ADI 2081) – Ion chromatography (Metrohm, 761Compact IC)) every 30 min. An aqueous solution comprising 9.67 mM of NaCO₃ and 2.47 mM of NaHCO₃ was used for anion eluent. A 2.0 mM HNO₃ aqueous solution was used as a cation eluent. A 4.6 μM LiBr solution was used as an internal standard for PILS-IC. Particle acidity was measured using a colorimetric integrated with a reflectance UV-visible spectrometer (C-RUV) which is developed by Jang et al. (2008).

Two days before the experiment, the chamber was flushed with the clean air using a clean air generator (GC Series, IQAir). Before sunrise, the gaseous compounds and aerosols in the background air inside the chamber were measured. The aromatic volatile organic compound (AVOC) (toluene or 135-TMB) was injected into the chamber using a glass chemical injector

under clean air stream. About 1 ppm of carbon tetrachloride (CCl_4) was also added to the chamber as a non-reactive tracer to account for dilution. Gaseous nitrous acid (HONO) that was synthesized through the reaction of 25 ml of 0.1 M NaNO_2 and 25 ml of 10 % H_2SO_4 in a conical flask was introduced into the chamber by passing the clean air stream through the flask. The initial concentration of NO_x including HONO, was measured using a chemiluminescence NO/NO_2 analyzer (Teledyne, model 200E) with molybdenum converter which can convert 100% of HONO to NO at 350 °C. The HONO concentration was measured by a difference in NO_x concentrations between with and without the denuder (1% Na_2CO_3 + 1% glycerol coated) that adsorbs HONO (Febo and Perrino, 1991). Sulfur dioxide (SO_2) was injected into the chamber from a tank of 500 ppm SO_2 . All gas (AVOC, CCl_4 , NO_x , O_3 and SO_2) and particle (OC/EC, particle distribution, aerosol inorganic ions and aerosol acidity) data were alternatively measured between the east and west chambers by switching sampling valves over the course of experiment.

Figure S2. Simulation of gas-phase oxidation of toluene and 135-TMB.



Time profiles of measured (symbols) and simulated (solid lines) concentrations of AVOCs, NO_x, and O₃ for toluene and 135-TMB under low and high NO_x conditions (A: Exp 01/06/12E, B: Exp 02/09/12E, C: Exp 05/20/12E, D: Exp 05/18/12E). For the toluene experiments (Figs. S2A, S2B), toluene decay, NO/NO₂ conversion and O₃ production are reasonably predicted, and for the 135-TMB experiments (Figs. S2C, S2D), 135-TMB decay and O₃ formation are reasonably estimated but NO₂+HONO concentrations (instrumentally, NO₂ measurement includes HONO) appear to decrease faster than measured concentrations after 09:00 EST. This may be partially explained by an instrumental artifact in that organic nitrate compounds are detected as NO₂ in the chemiluminescence NO_x analyzer.

Section S2. Description of the concentrations of organic compounds in aqueous phase

To describe the concentrations of organic compounds in the inorganic aqueous phase, the estimation of the gas-particle partition coefficient ($K_{in,i}$) of an organic compound between the gas and inorganic aerosol phases is necessary. $K_{in,i}$ is expressed as (Pankow, 1994),

$$K_{in,i} = \frac{7.501 RT}{10^9 MW_{in} \gamma_{in,i} p_{l,i}^o} \quad (S1)$$

where R is the gas constant ($8.314 \text{ J mol}^{-1} \text{ K}^{-1}$), T is the temperature (K), and MW_{in} is the average molecular weight (g mol^{-1}) of inorganic aerosols. $p_{l,i}^o$ is the sub-cooled liquid vapor pressure (mmHg) of compound, i . $\gamma_{in,i}$ is the activity coefficients of the organic compound, i in the inorganic phases. The concentrations of organic compounds in aqueous solution are affected by inorganic salt concentrations. Generally, less organic compounds are soluble in aqueous solutions with higher salt concentrations. To incorporate the solubility of organic compounds in atmospheric aerosols with different RH in the model, which usually contain inorganic salts, the activity coefficient of organic compounds should be calculated in salt water. However, there are currently no available thermodynamic models that can calculate the activity coefficient of organic compounds in salt water. Therefore, in this study, the activity coefficient of organic compounds in pure water is calculated first using Hansen's cohesive energies and solubility parameter method (Barton, 1991) and then corrected to the one in salted aqueous aerosol at 70% RH using the empirically obtained relationship of activity coefficients of organic compounds in pure water and in NaCl aqueous aerosol at 70% RH (literature solubility data of NaCl were used because of the lack of literature data for ammonia-sulfate aerosol) (Fig. S3 and Table S1). Each inorganic salt requires a certain amount of water to liquefy at the deliquesce relative humidity (DRH, solid to liquid). Similarly, when humidity drops from very high to DRH, salt will retain a certain amount of water until the efflorescence relative humidity (ERH) is reached. The majority of the water solubilities of organic compounds are available for low concentrations that correspond to high humidities. Thus, the activity coefficients of organic compounds in low concentration in water, which is related to 70% RH, are used to estimate the solubility of organic compounds in salt aerosols.

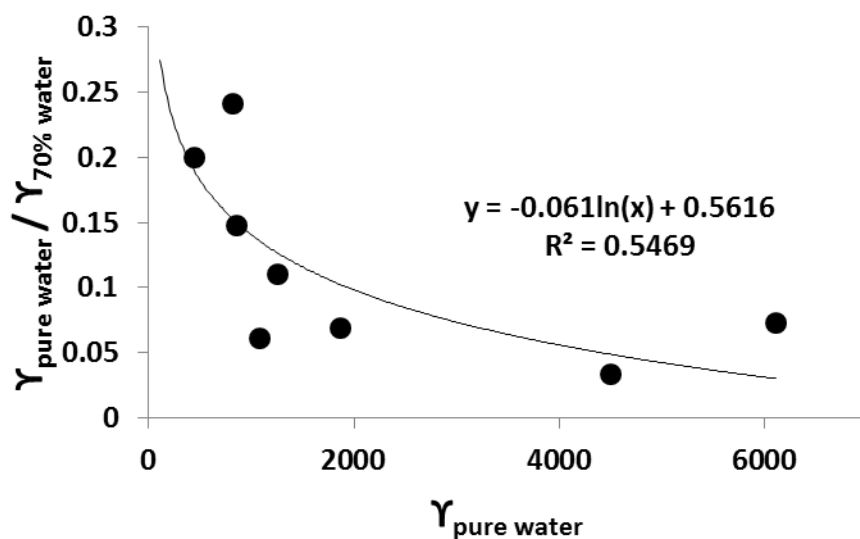


Figure S3. Regression of the activity coefficient ratio of organic compounds in pure water to NaCl salted water at 70% RH.

Table S1. Experimental activity coefficients of organic compounds in pure water and 30% NaCl salted water.

Compound	γ_{water}	$\gamma_{70\% \text{ water}}$	$\gamma_{70\% \text{ water}} / \gamma_{\text{water}}$	Reference
Vanillic acid	6,106	83,313	0.073	Noubigh et al., 2007
Pentyl acetate	4,503	133,430	0.033	Segatin and Klofutar, 2000
Ferulic acid	1,865	26,924	0.069	Noubigh et al., 2007
Phthalic acid	1,250	11,305	0.110	Bretti et al., 2005
Butyl acetate	1,078	17,556	0.061	Segatin and Klofutar, 2000
Vanillin	856	5,800	0.147	Noubigh et al., 2007
Gallic acid	818	3,391	0.241	Noubigh et al., 2007
Protocatechuic acid	449	2,252	0.199	Noubigh et al., 2007

Section S3. Derivation of analytical solution of ΔOM_{AR}

For convenience, all equations in the supporting information are numbered independently from the manuscript, although some equations are shown in the manuscript.

The partitioning coefficients of lumping species, i between gas (g) and two condensed phases (organic phase, or and inorganic phase, in) can be expressed using $K_{or,i}$ ($m^3 \mu g^{-1}$, $g \leftrightarrow or$) and $K_{in,i}$ ($m^3 \mu g^{-1}$, $g \leftrightarrow in$).

$$K_{or,i} = \frac{C_{or,i}}{C_{g,i} OM_T} \quad (S2)$$

$$K_{in,i} = \frac{C_{in,i}}{C_{g,i} M_{in}} \quad (S3)$$

where $C_{g,i}$, $C_{or,i}$ and $C_{in,i}$ are concentrations ($\mu g m^{-3}$ of air) of lumping species, i in the gas, organic and inorganic aerosol phases, respectively. OM_T is the total organic aerosol mass concentration ($\mu g m^{-3}$) and M_{in} is the inorganic aerosol mass concentration ($\mu g m^{-3}$).

The concentrations of each lumping species in the gas, organic aerosol, and inorganic aerosol-phases are derived from the Eqs. (S2) and (S3).

$$C_{g,i} = \frac{1}{1+K_{or,i}OM_T+K_{in,i}M_{in}} C_{T,i} \quad (S4)$$

$$C_{or,i} = \frac{K_{or}OM_T}{1+K_{or,i}OM_T+K_{in,i}M_{in}} C_{T,i} \quad (S5)$$

$$C_{in,i} = \frac{K_{in}M_{in}}{1+K_{or,i}OM_T+K_{in,i}M_{in}} C_{T,i} \quad (S6)$$

where $C_{T,i}$ ($\mu g m^{-3}$, $C_{T,i} = C_{g,i} + C_{or,i} + C_{in,i}$) is the total concentration of lumping species, i .

In the UNIPAR model, organic matter (ΔOM_{AR}) formed by aerosol phase reactions are described by two processes, the oligomerization in the organic phase and acid-catalyzed reaction

in the inorganic phase. The reactions in both the phases are derived based on a second order kinetic self-dimerization reaction.

$$\frac{dC'_{or,i}}{dt} = -k_{o,i}C'_{or,i}{}^2 \quad (\text{In the organic phase}) \quad (\text{S7}) \quad [\text{Eq. (7) in the manuscript}]$$

$$\frac{dC'_{in,i}}{dt} = -k_{AC,i}C'_{in,i}{}^2 \quad (\text{In the inorganic phase}) \quad (\text{S8}) \quad [\text{Eq. (8) in the manuscript}]$$

where $C'_{or,i}$ and $C'_{in,i}$ are the aerosol-based concentration of lumping species, i (mol L^{-1}). $k_{o,i}$ is the 2nd order reaction rate constant ($\text{L mol}^{-1} \text{s}^{-1}$) for oligomerization of lumping species, i in the organic phase. $k_{AC,i}$ is the 2nd order reaction rate constant ($\text{L mol}^{-1} \text{s}^{-1}$) for acid-catalyzed reaction of lumping species, i in the inorganic phase. Aerosol based concentration $C'_{x,i}$ (mol L^{-1}) and air-based concentration $C_{x,i}$ ($\mu\text{g m}^{-3}$) ($x=or, in$) can be converted by unit conversion factor $f_{or,i}$ and $f_{in,i}$, defined as follow.

$$f_{or,i} = \frac{C_{or,i}}{C'_{or,i}} = \left(\frac{MW_i \cdot OM_T}{\rho_{or} 10^3} \right) \quad (\text{S9})$$

$$f_{in,i} = \frac{C_{in,i}}{C'_{in,i}} = \left(\frac{MW_i \cdot M_{in}}{\rho_{in} 10^3} \right) \quad (\text{S10})$$

where MW_i is the molecular weight of lumping species i . ρ_{or} and ρ_{in} are the densities of the organic phase and inorganic phase.

The amount of OM formed by the aerosol phase reactions (ΔOM_{AR}) is same as the amount of consumed total concentrations ($C_{T,i}$) of lumping species based on a mass balance.

Therefore, the ΔOM_{AR} can be expressed as

$$\Delta OM_{AR} = -\sum_i \Delta C_{T,i} = -\sum_i \int dC_{T,i} \quad (\text{S11}) \quad (\text{Eq. (10) in the manuscript})$$

To solve Eq. (S11), all of partitioning and aerosol phase reactions in the multi-phase system are kinetically described. (Fig. (S4))

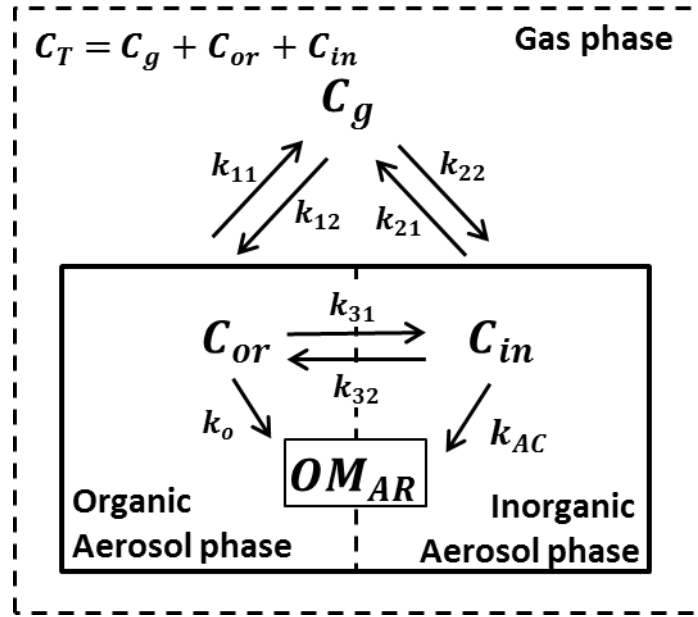


Figure S4. Kinetic scheme for SOA formation in the UNIPAR model.

Kinetic expressions of lumping components are shown in following equations.

$$\frac{dC_{g,i}}{dt} = k_{11}C_{or,i} - k_{12}C_{g,i} + k_{21}C_{in,i} - k_{22}C_{g,i} \quad (S12)$$

$$\frac{dC_{or,i}}{dt} = -k_{11}C_{or,i} + k_{12}C_{g,i} - k_{31}C_{or,i} + k_{32}C_{in,i} - k_{o,i}C_{or,i}^2 f_{or,i} \quad (S13)$$

$$\frac{dC_{in,i}}{dt} = -k_{21}C_{in,i} + k_{22}C_{g,i} + k_{31}C_{or,i} - k_{32}C_{in,i} - k_{AC,i}C_{in,i}^2 f_{in,i} \quad (S14)$$

where k_{nm} are first order reaction rate constants ($n, m=1-3, s^{-1}$), in which each pair of them represents equilibrium among $C_{g,i}$, $C_{or,i}$ and $C_{in,i}$.

From Eqs. (S12)–(S14), $\frac{dC_{T,i}}{dt}$ can be expressed as follow,

$$\frac{dC_{T,i}}{dt} = \frac{dC_{g,i}}{dt} + \frac{dC_{or,i}}{dt} + \frac{dC_{in,i}}{dt} = -k_{o,i}C_{or,i}^2 f_{or,i} - k_{AC,i}C_{in,i}^2 f_{in,i} \quad (S15)$$

Using the Eqs. (S5), (S6), (S9), and (S10), Eq. (S15) can be rearranged with respect to $C_{T,i}$.

$$\frac{dC_{T,i}}{dt} = - \left(k_{o,i} \frac{OM_T 10^3 \rho_{or} K_{or,i}^2}{MW_i (1 + K_{or,i} OM_T + K_{in,i} M_{in})^2} + k_{AC,i} \frac{M_{in} 10^3 \rho_{in} K_{in,i}^2}{MW_i (1 + K_{or,i} OM_T + K_{in,i} M_{in})^2} \right) C_{T,i}^2 \quad (S16)$$

Assuming the parameters in Eq. (S16), such as OM_T , M_{in} , and $k_{AC,i}$ are constants during computational time interval ($\Delta t=3$ min), Eq (S16) can be integrated as a general second order differential equation.

$$\Delta OM_{AR} = -\sum_i \int dC_{T,i} = -\sum_i \int_0^{\Delta t} (k_{o,i}\beta_{1,i} + k_{AC,i}\beta_{2,i})C_{T,i}^2 dt \quad (S17)$$

$$\text{where } \beta_{1,i} = \frac{OM_T 10^3 \rho_{or} K_{or,i}^2}{MW_i(1+K_{or,i} OM_T + K_{in,i} M_{in})^2}$$

$$\beta_{2,i} = \frac{M_{in} 10^3 \rho_{in} K_{in,i}^2}{MW_i(1+K_{or,i} OM_T + K_{in,i} M_{in})^2}$$

Then the analytical solution of ΔOM_{AR} can be obtained.

$$\Delta OM_{AR} = -\Delta C_{T,i} = \sum_i \frac{(k_{o,i}\beta_{1,i} + k_{AC,i}\beta_{2,i}) C_{T,i}^2 \Delta t}{1 + (k_{o,i}\beta_{1,i} + k_{AC,i}\beta_{2,i}) C_{T,i} \Delta t} \quad (S18)$$

Section S4. Description of the formation of organosulfate.

Parameter (N_{OS}) to count functional groups involved in OS formation. N_{OS} accounts for aldehyde, epoxide, and alcohol in this study. These functional groups are related to the reactivity of lumping groups. Fast [F] and medium [M] reactivity groups have two and one aldehyde or epoxide functional groups, respectively. Each aldehyde can react with two sulfate ion positions (Liggio and Li, 2006). Therefore, fast reactivity groups have a weighting factor of 4, and medium reactivity groups have a weighting factor of 2 in the model. For the multi-alcohol [MA] groups, the least volatile group ($i=1$) has a weighting factor of 4, and the second and third less volatile groups ($i=2$ and 3) use a weighting factor of 3.

$$N_{OS} = \sum_{i=1}^{30} w_i \cdot \Delta OM'_{AC,i} \quad (\text{S19})$$

w_i is the weighting factor that numerically estimate the capability of each lumping group for the formation of OS. $\Delta OM'_{AC,i}$ is the molar concentration ($\mu\text{mol m}^{-3}$) of OM formed through acid-catalyzed reaction of each lumping group, i in the inorganic phase during Δt .

Table S2. Weighting factor (w_i) of each lumping group for the calculation of the number of OS-formable functional groups, N_{OS}

w_i		Volatility (vapor pressure)					
		i=1 (10^{-8} mmHg)	i=2 (10^{-6} mmHg)	i=3 (10^{-5} mmHg)	i=4 (10^{-4} mmHg)	i=5 (10^{-3} mmHg)	i=6 (10^{-2} mmHg)
Reactivity	F	4	4	4	4	4	4
	M	2	2	2	2	2	2
	S	–	–	–	–	–	–
	P	–	–	–	–	–	–
	MA	4	3	3	–	–	–

Empirical parameter (f_{OS}) to estimate OS formation. The change of aerosol acidity due to the formation of OS can be experimentally estimated by comparison of the proton concentration ($[H^+]$) from the PILS-IC measurement and the C-RUV measurement. The PILS-IC measurement provides ion concentrations, such as ammonium and sulfate, and the $[H^+]$ of aerosol can be calculated using an aerosol thermodynamic model (E-AIM II). For ammonia-rich aerosols ($[\text{NH}_4^+]/[\text{total sulfate}] \geq 1$), the $[H^+]$ was estimated from the empirical data by Li and

Jang (2012). The C-RUV method directly measures the $[H^+]$ of aerosols by collecting the aerosol on a metanil yellow dyed filter, which changes color from yellow to pink in acidic conditions, and subsequently measuring the filter color change using reflectance UV-Visible spectrometry. By comparing the proton concentrations from PILS-IC measurement with C-RUV measurement, acidity change by OS formation can be estimated. For this study, the chamber experiment (06/20/12E) was conducted for the toluene and NO_x system with sulfuric acid seeds. The resulting proton concentrations are shown in Fig. S3. Then, the OS formation parameter f_{OS} (0.017) in Eq. (S14) was obtained by fitting the modeled proton concentration to the C-RUV measured concentration.

$$OS \text{ conversion factor} = \frac{[SO_4^{2-}]_{old} - [SO_4^{2-}]_{new}}{[SO_4^{2-}]_{old}} = \frac{\Delta OS}{[SO_4^{2-}]_{old}} = 1 - \frac{1}{1 + f_{OS} \cdot \frac{N_{OS}}{[SO_4^{2-}]_{free}}}$$

(S20) (Eq. (12) in the manuscript)

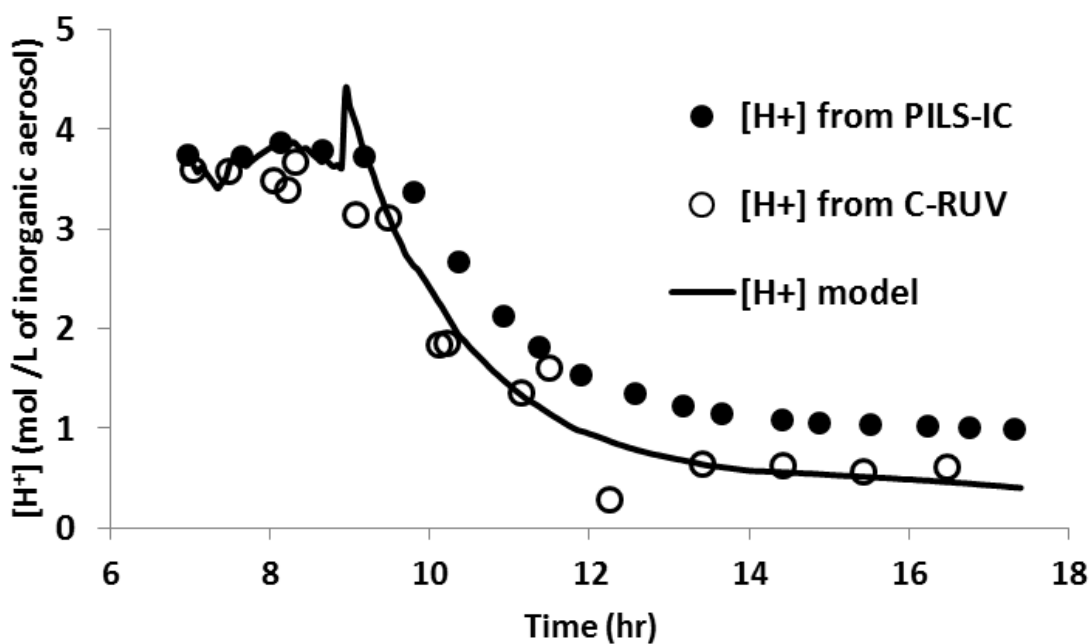


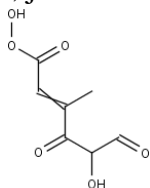
Figure S5. Time profile of aerosol proton concentration for the toluene experiment with sulfuric acid seeds.

Section S5. Lumping of gas phase oxidation products

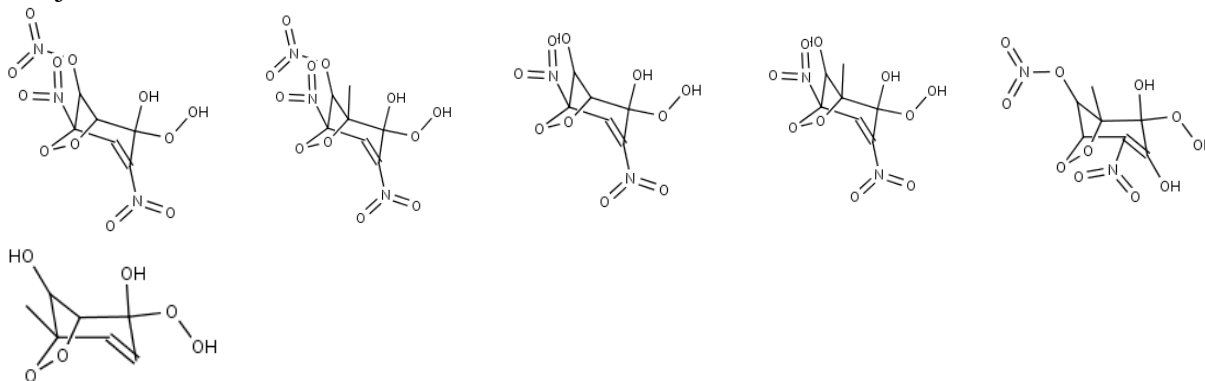
Vapor pressures of model-predicted photooxidation products are estimated as a function of boiling point and entropy of vaporization (detailed method is described in elsewhere (Cao and Jang, 2010; Jang and Kamens, 2001)). The reactivity for aerosol phase reaction is determined based on products' functional groups: the product containing more than two aldehyde or epoxide functional groups is categorized into group F, the product containing an aldehyde or epoxide functional groups is for group M, the product containing ketone functional groups is for group S, and the product without those functional groups is for group P. Among the group P, the products with more than three of alcohol functional groups are designated to group MA, which is later used for the estimation of organosulfates with other reactive products (see section “*organosulfate formation*”).

Figure S6. The list of the products in each lumping group for toluene oxidation (*i* denotes volatility and *j* denotes reactivity of organic compounds in 30 lumping groups)

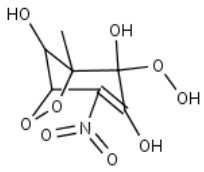
$i=1, j=M$



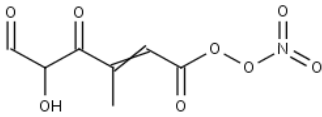
$i=1, j=P$



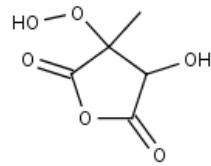
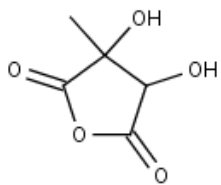
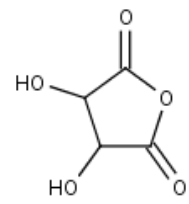
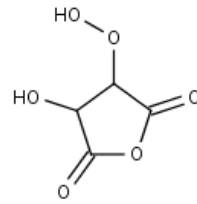
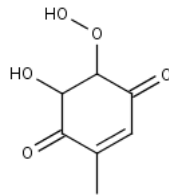
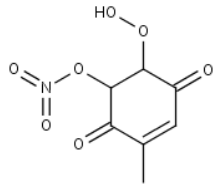
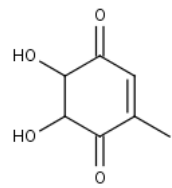
$i=1, j=MA$



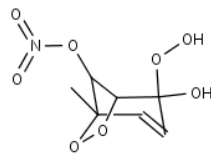
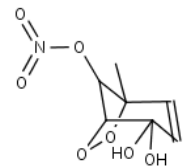
$i=2, j= M$



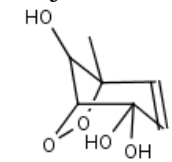
$i=2, j= S$



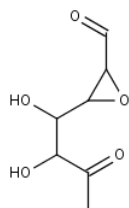
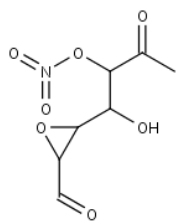
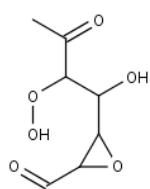
$i=2, j= P$



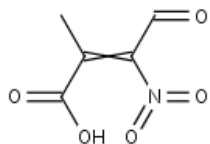
$i=2, j= MA$



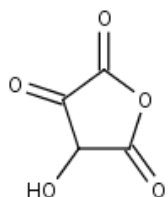
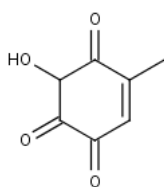
$i=3, j= F$



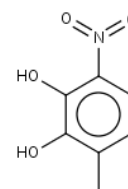
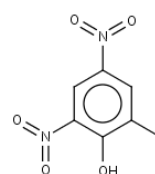
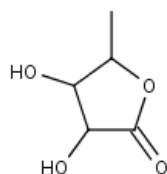
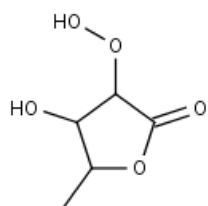
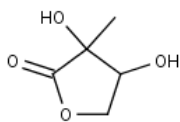
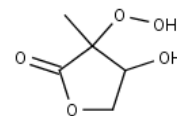
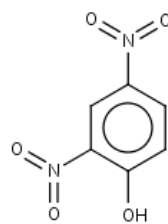
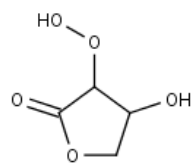
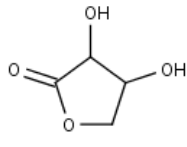
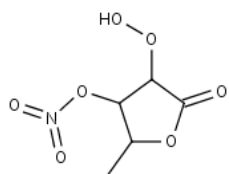
$i=3, j= M$



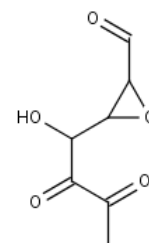
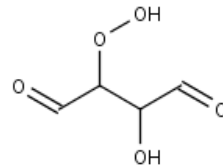
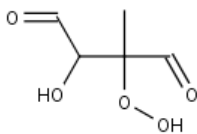
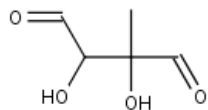
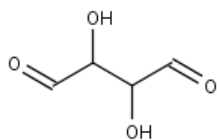
$i=3, j= S$



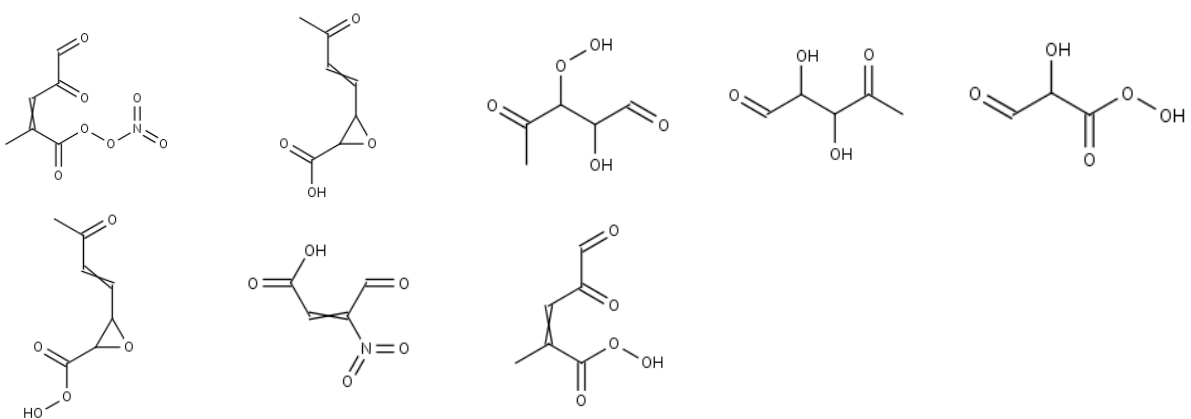
$i=3, j= P$



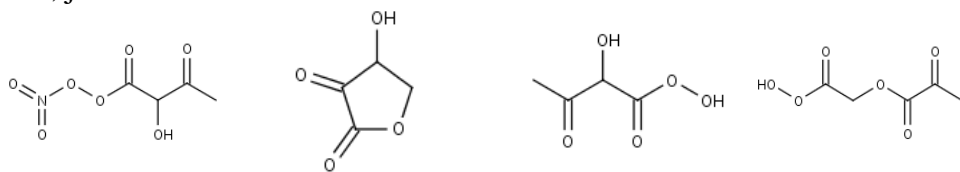
$i=4, j= F$



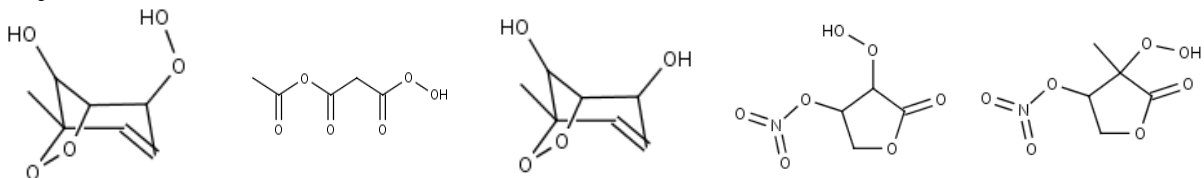
$i=4, j= M$



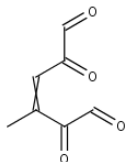
i=4, j= S



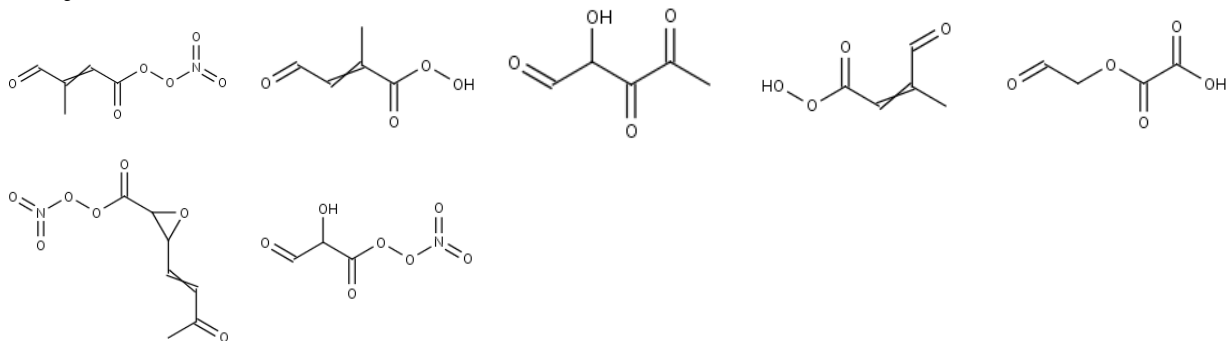
i=4, j= P



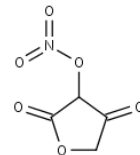
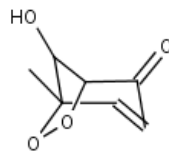
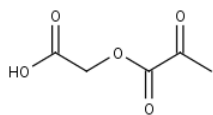
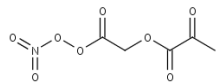
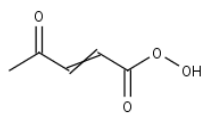
i=5, j= F



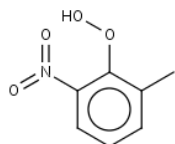
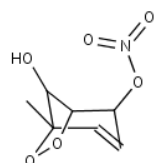
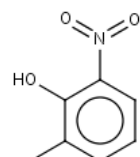
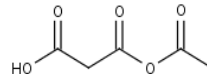
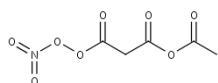
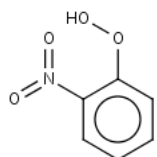
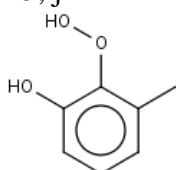
i=5, j= M



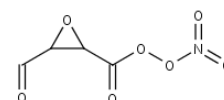
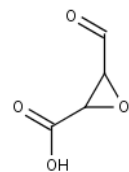
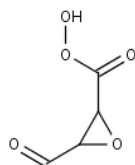
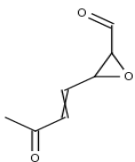
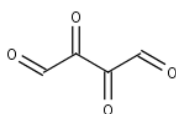
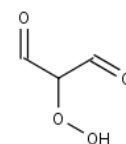
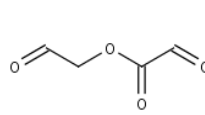
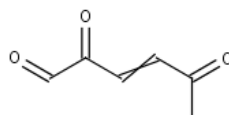
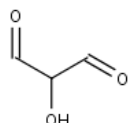
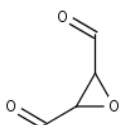
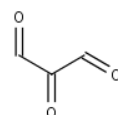
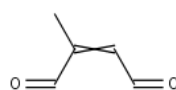
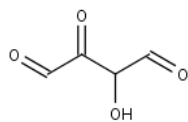
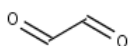
$i=5, j= S$



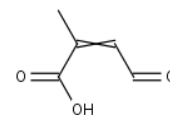
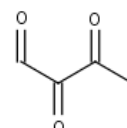
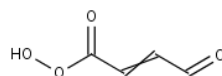
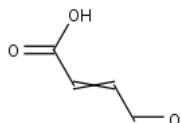
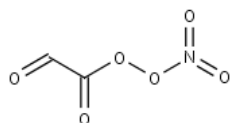
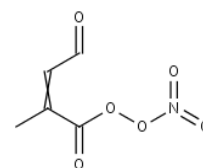
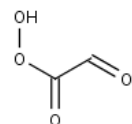
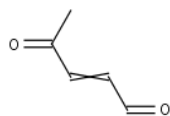
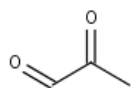
$i=5, j= P$

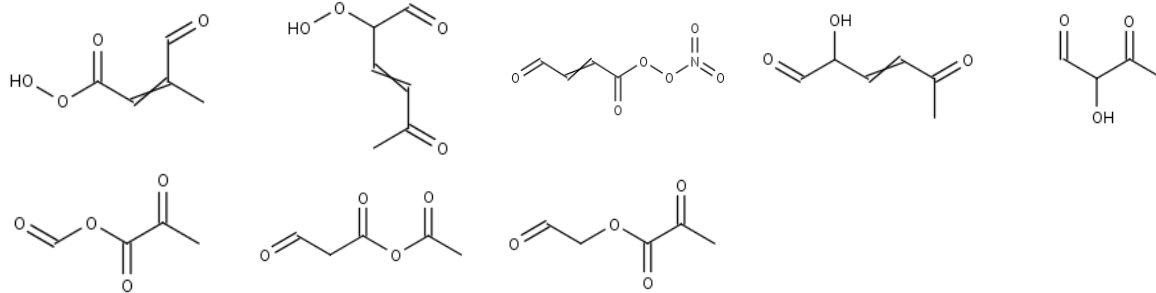


$i=6, j= F$

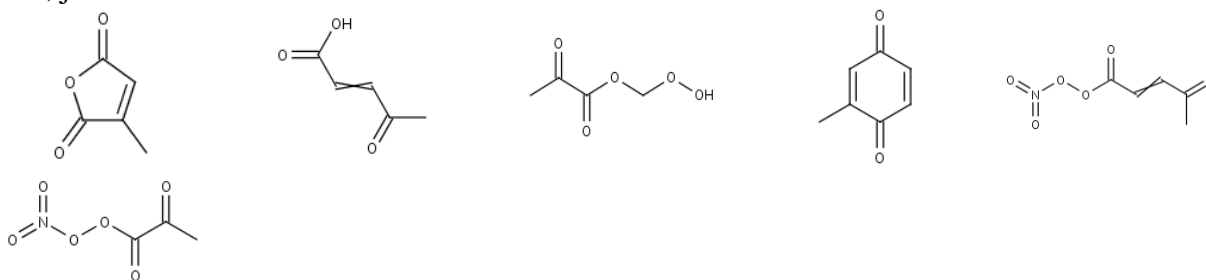


$i=6, j= M$





i=6, j= S



i=6, j= P

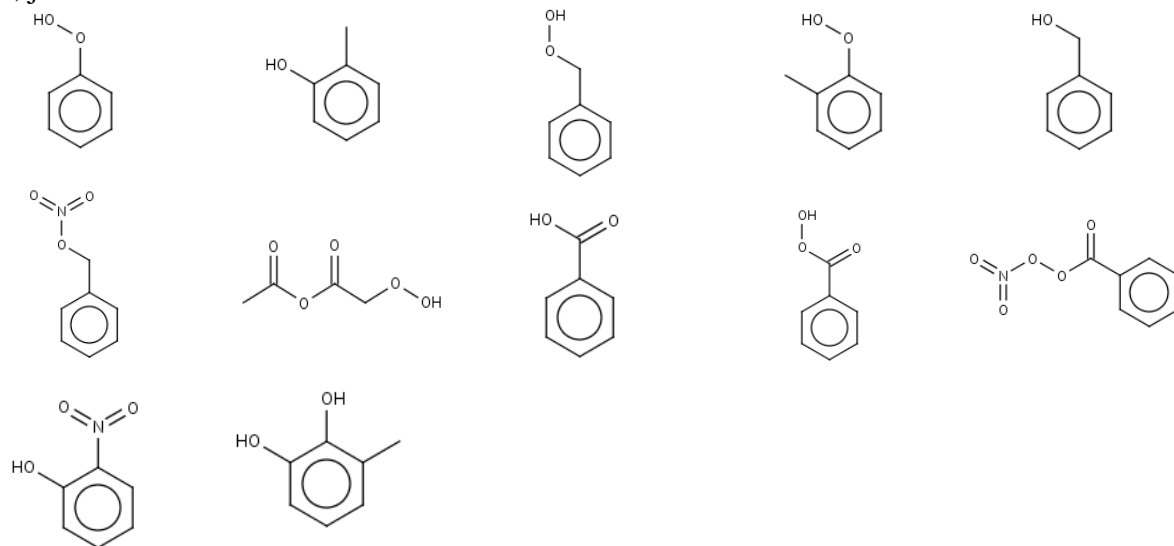
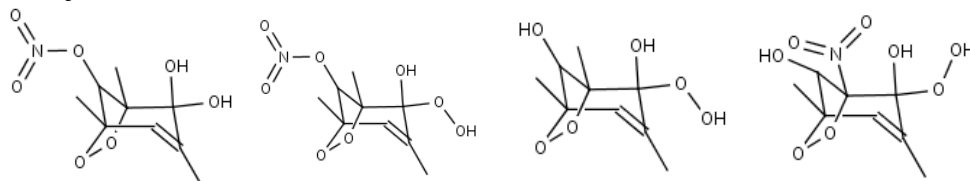
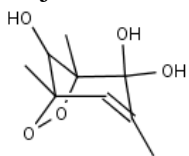


Figure S7. The list of the products in each lumping group for 1, 3, 5 - trimethylbenzene oxidation (*i* and *j* denote volatility and reactivity of organic compounds in 30 lumping groups, respectively)

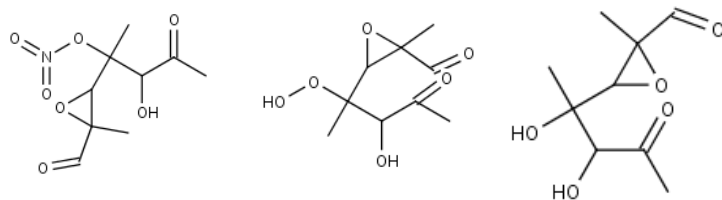
i=1, *j*= P



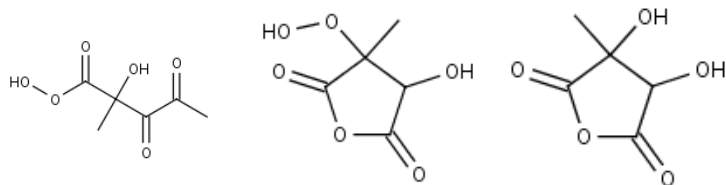
i=2, *j*= A



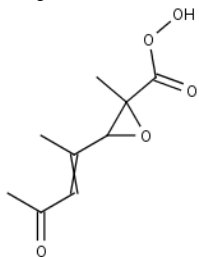
i=2, *j*= F



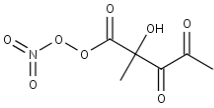
i=2, *j*= S



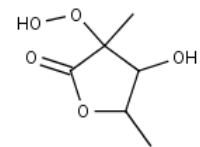
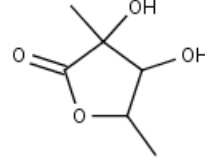
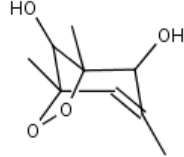
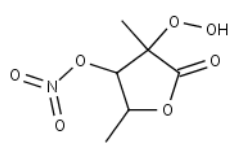
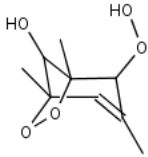
i=3, *j*= M



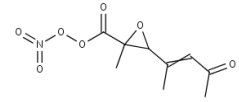
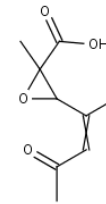
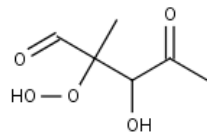
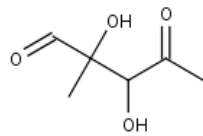
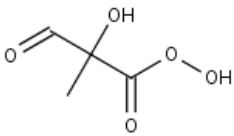
i=3, *j*= S



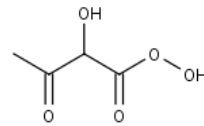
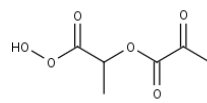
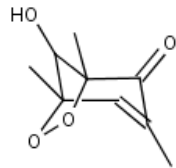
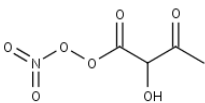
i=3, j= P



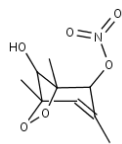
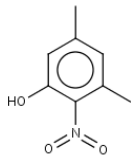
i=4, j= M



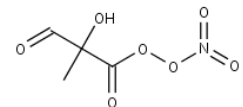
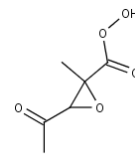
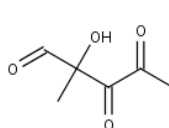
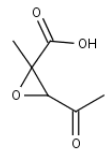
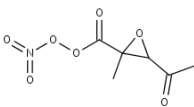
i=4, j= S



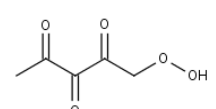
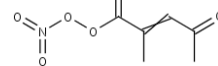
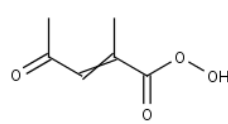
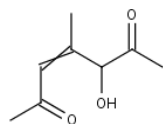
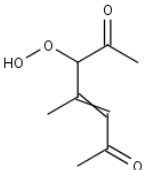
i=4, j= P

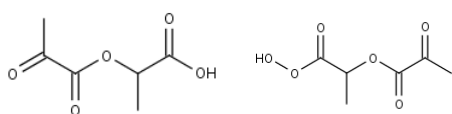


i=5, j= M

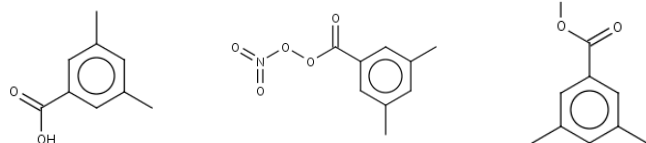


i=5, j= S

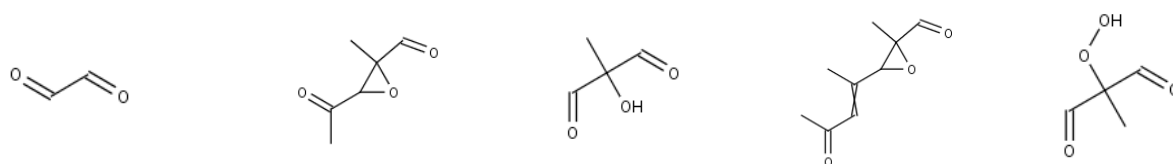




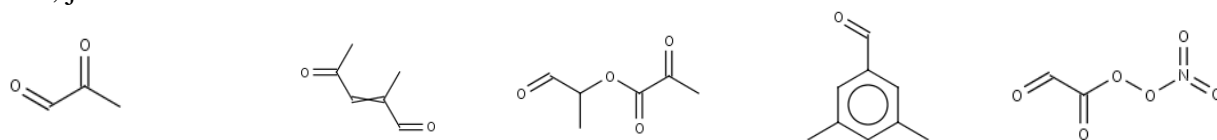
$i=5, j=P$



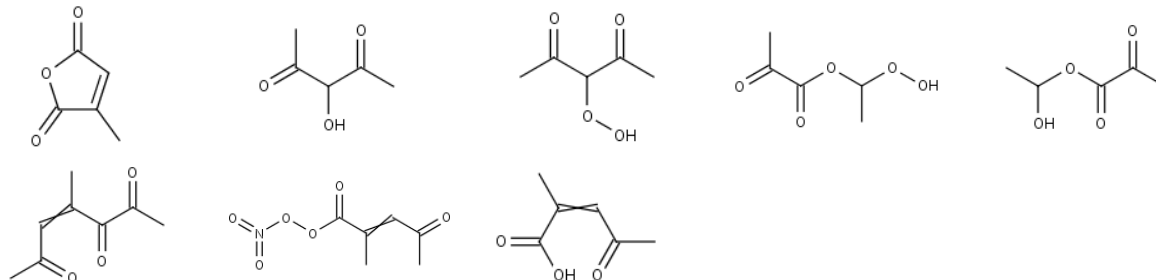
$i=6, j=F$



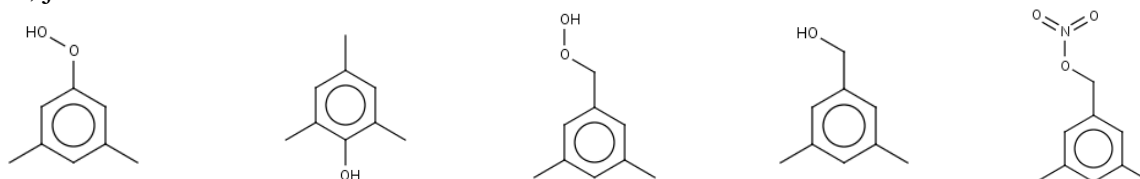
$i=6, j=M$



$i=6, j=S$



$i=6, j=P$



Section S6. NO_x dependency of the stoichiometric coefficient matrix

To consider the effect of NO_x on SOA formation, mass based product stoichiometric coefficients ($\alpha_{i,j}$) are evaluated in various NO_x conditions using gas-phase kinetic model (MCM V3.2). Toluene or 135TMB are simulated in several VOC/NO_x conditions (ppbC/ppb) (Tables S3 and S4) and regression equations are obtained as a function of VOC/NO_x ratio. In simulation, one of clear day's meteorological conditions (January 06, 2012) are used (Fig. S8) and same artificial OH radical sources are added in mechanisms like other chamber simulations. $\alpha_{i,j}$ matrix is determined when the precursor is consumed half of total consumption during the experiment ($\Delta\text{ROG}/2$) as a representative. The resulting regression equations of $\alpha_{i,j}$ for toluene and 135 TMB are shown in Tables S5 and S6.

Table S3. Simulation conditions for the evaluation of product stoichiometric coefficient, $\alpha_{i,j}$ for toluene oxidation.

	1	2	3	4	5	6	7	8	9
Toluene (ppb)	200	200	200	200	200	200	200	200	200
NO _x (ppb)	20	30	40	70	100	150	200	250	300
VOC/NO _x (ppbC/ppb)	70	46.7	35	20	14	9.3	7	5.6	4.7

Table S4. Simulation conditions for the evaluation of product stoichiometric coefficient, $\alpha_{i,j}$ for 135-TMB oxidation.

	1	2	3	4	5	6	7	8	9
135-TMB (ppb)	200	200	200	200	200	200	200	200	200
NO _x (ppb)	20	30	40	70	100	150	200	300	400
VOC/NO _x (ppbC/ppb)	90	60	45	25.7	18	12	9	6	4.5

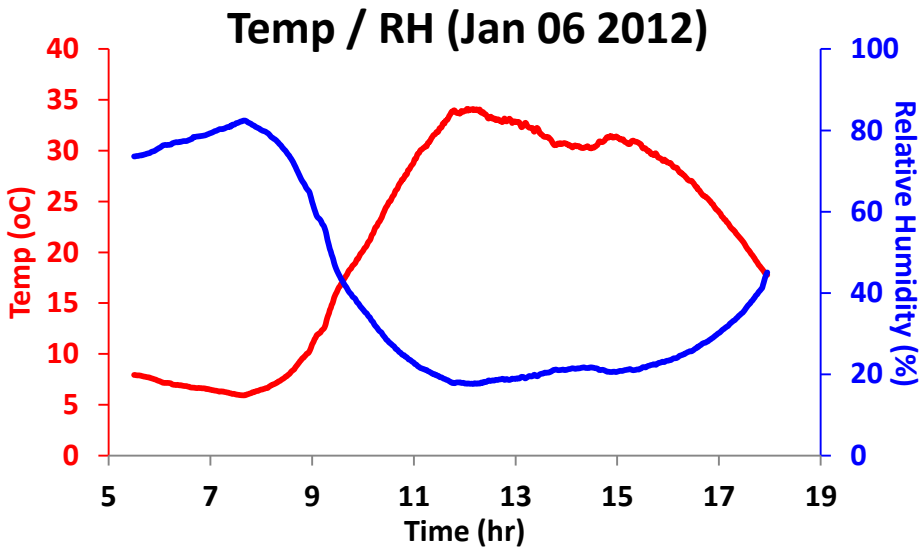
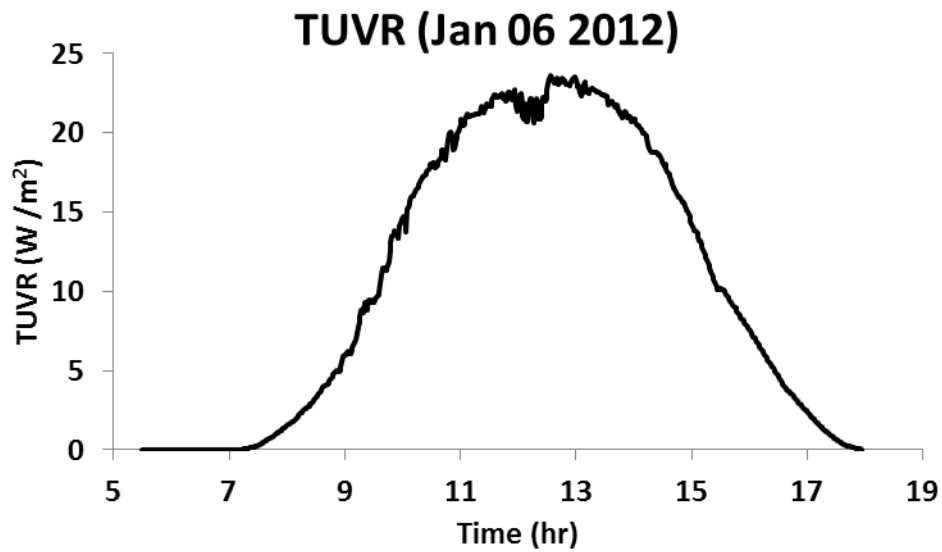


Figure S8. Time profile of sunlight total ultra-violet radiation (TUVR) and temperature and relative humidity measured in the UF-APHOR east chamber on January 06, 2012.

Table S5. Regression equations of the product stoichiometric coefficients ($\alpha_{i,j}$) as functions of VOC/NO_x (ppbC/ppb) ratio for toluene.

X ≤ 14^a [X=VOC/NO _x]	
α (F,1) ^b	0
α (F,2)	0
α (F,3)	$3.756098E-07x^3 + 1.988549E-05x^2 - 9.464828E-05x + 3.475627E-03$
α (F,4)	$1.094572E-07x^3 + 8.926093E-06x^2 - 1.492385E-05x + 1.030460E-03$
α (F,5)	$2.464277E-07x^3 - 1.346271E-05x^2 + 1.911749E-04x - 4.587156E-04$
α (F,6)	$2.602796E-05x^3 - 1.124175E-03x^2 + 1.765939E-02x + 2.046016E-01$
α (M,1)	0
α (M,2)	$1.388478E-06x^3 - 4.305879E-05x^2 + 4.213540E-04x + 4.365794E-04$
α (M,3)	$7.977641E-05x^3 - 2.790630E-03x^2 + 3.021985E-02x - 5.135372E-02$
α (M,4)	$-7.831470E-08x^3 + 5.560318E-06x^2 - 3.513139E-05x + 7.866549E-05$
α (M,5)	$1.240897E-05x^3 - 3.976363E-04x^2 + 4.676057E-03x + 4.917202E-03$
α (M,6)	$5.119742E-05x^3 - 1.951616E-03x^2 + 2.712552E-02x + 2.174854E-01$
α (S,1)	0
α (S,2)	$-2.669237E-07x^3 + 9.259240E-06x^2 - 7.221154E-05x + 1.657688E-04$
α (S,3)	0
α (S,4)	$5.761599E-06x^3 - 2.335165E-04x^2 + 3.159902E-03x - 2.600717E-03$
α (S,5)	$4.861152E-06x^3 - 1.234912E-04x^2 + 1.792228E-03x + 2.012876E-02$
α (S,6)	$4.103202E-05x^3 - 1.248161E-03x^2 + 1.270531E-02x + 4.950428E-02$
α (P,1)	$-6.401555E-06x^3 + 2.084480E-04x^2 - 1.613352E-03x + 3.692384E-03$
α (P,2)	$-1.882975E-06x^3 + 6.725052E-05x^2 - 5.358991E-04x + 1.247308E-03$
α (P,3)	$-1.141182E-04x^3 + 4.072313E-03x^2 - 4.571298E-02x + 2.156422E-01$
α (P,4)	$-4.847070E-06x^3 + 2.594583E-04x^2 - 2.185684E-03x + 5.173091E-03$
α (P,5)	$1.295314E-04x^3 - 4.684761E-03x^2 + 5.571233E-02x - 1.947936E-02$
α (P,6)	$-6.342056E-05x^3 + 2.190472E-03x^2 - 2.340949E-02x + 1.422797E-01$
α (MA,1)	$-1.371906E-07x^3 + 1.234486E-05x^2 - 1.049651E-04x + 2.460212E-04$
α (MA,2)	0
α (MA,3)	0
α (MA,4)	0
α (MA,5)	0
α (MA,6)	0
X > 14	
α (F,1)	0
α (F,2)	0
α (F,3)	$4.374686E-09x^3 - 2.549720E-06x^2 + 3.255410E-04x + 9.459666E-04$

α (F,4)	$1.875327E-08x^3 - 3.597563E-06x^2 + 3.094367E-04x - 1.414916E-03$
α (F,5)	$-4.059367E-09x^3 + 6.464917E-07x^2 - 3.408290E-05x + 6.157527E-04$
α (F,6)	$-4.255417E-08x^3 + 1.325569E-05x^2 - 2.378351E-03x + 3.343833E-01$
α (M,1)	0
α (M,2)	$8.696286E-10x^3 + 4.624925E-08x^2 - 3.002746E-05x + 2.119281E-03$
α (M,3)	$-2.635015E-07x^3 + 4.936192E-05x^2 - 3.237349E-03x + 8.018525E-02$
α (M,4)	$1.064408E-08x^3 - 1.990596E-06x^2 + 1.411371E-04x - 1.149206E-03$
α (M,5)	$1.078369E-09x^3 - 5.115752E-06x^2 + 3.204545E-04x + 2.308144E-02$
α (M,6)	$1.047000E-07x^3 - 2.042259E-05x^2 - 9.472423E-04x + 3.729465E-01$
α (S,1)	0
α (S,2)	$1.094797E-08x^3 - 1.638750E-06x^2 + 8.648740E-05x - 6.792252E-04$
α (S,3)	$5.485777E-09x^3 - 8.352996E-07x^2 + 4.640720E-05x - 3.977676E-04$
α (S,4)	$3.995721E-08x^3 - 4.595782E-06x^2 + 3.450665E-05x + 1.205253E-02$
α (S,5)	$-3.588602E-09x^3 - 1.724619E-06x^2 + 1.707153E-03x + 1.060108E-02$
α (S,6)	$-7.194779E-08x^3 + 6.953575E-07x^2 + 5.909469E-04x + 8.713093E-02$
α (P,1)	$-2.077924E-06x^2 + 2.799649E-04x + 1.998606E-03$
α (P,2)	$1.270294E-07x^3 - 1.838457E-05x^2 + 7.820065E-04x - 5.847066E-03$
α (P,3)	$4.446063E-07x^3 - 8.343187E-05x^2 + 5.250710E-03x + 1.852973E-03$
α (P,4)	$-9.379561E-08x^3 - 6.258217E-06x^2 + 3.343902E-03x - 3.338632E-02$
α (P,5)	$9.361983E-08x^3 + 2.824535E-06x^2 - 2.513297E-03x + 2.328965E-01$
α (P,6)	$-1.090433E-07x^3 - 3.667089E-06x^2 + 2.155964E-03x + 4.024704E-02$
α (MA,1)	$3.011409E-08x^3 - 6.061746E-06x^2 + 4.190061E-04x - 3.992835E-03$
α (MA,2)	0
α (MA,3)	0
α (MA,4)	0
α (MA,5)	0
α (MA,6)	0

^a x is the ratio of VOC to NO_x (VOC/NO_x, ppbC/ppb)

^b In α (j, i), j denotes heterogeneous reactivity (fast (F), medium (M), slow (S), partitioning only (P), multi-alcohol (MA)) and i denotes volatility (vapor pressure) (10^{-8} (1), 10^{-6} (2), 10^{-5} (3), 10^{-4} (4), 10^{-3} (5), 10^{-2} (6)) (mmHg) of lumping structure.

Table S6. Regression equations of product stoichiometric coefficients ($\alpha_{i,j}$) as functions of VOC/NO_x (ppbC/ppb) ratio for 135-TMB.

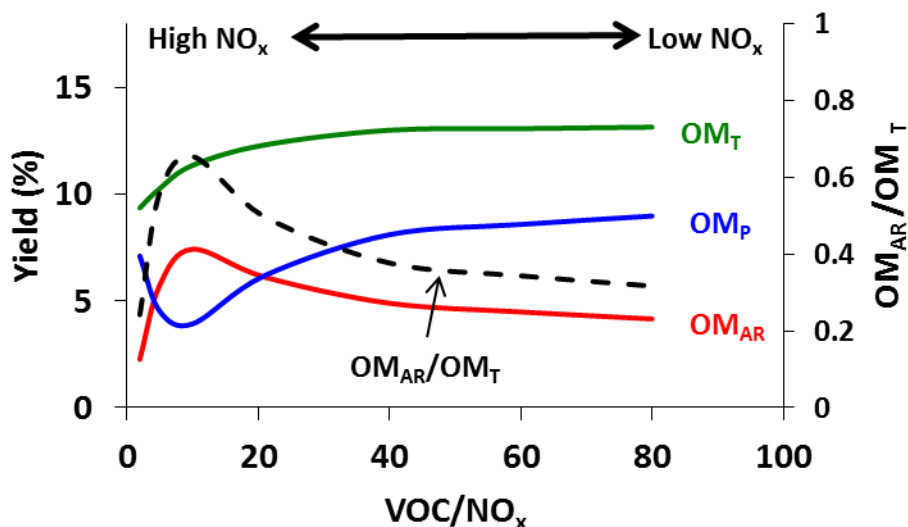
X ≤ 26^a [X=VOC/NO _x]	
α (F,1) ^b	0
α (F,2)	$-1.227911\text{E-}06x^3 + 6.041205\text{E-}05x^2 - 4.262702\text{E-}04x + 4.878133\text{E-}03$
α (F,3)	0
α (F,4)	0
α (F,5)	0
α (F,6)	$8.072754\text{E-}07x^3 - 4.550916\text{E-}05x^2 + 7.093282\text{E-}04x + 5.174296\text{E-}02$
α (M,1)	0
α (M,2)	0
α (M,3)	0
α (M,4)	$1.002901\text{E-}07x^3 - 1.840011\text{E-}05x^2 + 7.000418\text{E-}04x + 5.024315\text{E-}03$
α (M,5)	$8.995901\text{E-}08x^3 - 1.222420\text{E-}05x^2 + 3.131691\text{E-}04x + 3.411166\text{E-}03$
α (M,6)	$6.557296\text{E-}05x^3 - 3.893436\text{E-}03x^2 + 5.348025\text{E-}02x + 4.966272\text{E-}01$
α (S,1)	0
α (S,2)	0
α (S,3)	0
α (S,4)	$-4.714006\text{E-}06x^3 + 2.603582\text{E-}04x^2 - 2.217035\text{E-}03x + 6.882090\text{E-}02$
α (S,5)	$1.208740\text{E-}06x^3 - 1.019662\text{E-}04x^2 + 2.484113\text{E-}03x + 3.371555\text{E-}03$
α (S,6)	$7.474346\text{E-}07x^3 - 1.214366\text{E-}04x^2 + 4.386343\text{E-}03x + 1.943249\text{E-}01$
α (P,1)	$-8.342084\text{E-}07x^3 + 4.933388\text{E-}05x^2 - 4.153890\text{E-}04x + 9.794614\text{E-}04$
α (P,2)	0
α (P,3)	$-1.277000\text{E-}05x^3 + 7.332458\text{E-}04x^2 - 6.268319\text{E-}03x + 1.489738\text{E-}02$
α (P,4)	$1.508863\text{E-}06x^3 - 7.368442\text{E-}05x^2 + 4.589595\text{E-}04x + 7.449735\text{E-}02$
α (P,5)	$1.973656\text{E-}07x^3 - 1.415763\text{E-}05x^2 + 2.755715\text{E-}04x + 2.173602\text{E-}03$
α (P,6)	$-3.453330\text{E-}06x^3 + 2.165122\text{E-}04x^2 - 3.785732\text{E-}03x + 3.098696\text{E-}02$
α (MA,1)	0
α (MA,2)	0
α (MA,3)	0
α (MA,4)	0
α (MA,5)	0
α (MA,6)	0
X > 26	
α (F,1)	0
α (F,2)	$8.370587\text{E-}08x^3 - 1.626103\text{E-}05x^2 + 9.931609\text{E-}04x - 3.221591\text{E-}03$
α (F,3)	0

α (F,4)	0
α (F,5)	0
α (F,6)	$-6.137160E-08x^3 + 1.298385E-05x^2 - 9.557081E-04x + 7.062714E-02$
α (M,1)	0
α (M,2)	0
α (M,3)	0
α (M,4)	$-3.119463E-08x^3 + 7.433847E-06x^2 - 6.344631E-04x + 2.449157E-02$
α (M,5)	$-2.679114E-08x^3 + 5.432713E-06x^2 - 3.687925E-04x + 1.126819E-02$
α (M,6)	$-4.178558E-06x^3 + 8.566464E-04x^2 - 5.783947E-02x + 1.403961E+00$
α (S,1)	0
α (S,2)	0
α (S,3)	0
α (S,4)	$1.784895E-07x^3 - 4.979452E-05x^2 + 5.767749E-03x - 1.460586E-02$
α (S,5)	$9.955961E-08x^3 - 1.991214E-05x^2 + 1.247024E-03x - 1.382325E-04$
α (S,6)	$-5.167016E-07x^3 + 1.188983E-04x^2 - 9.669114E-03x + 4.183827E-01$
α (P,1)	$4.446401E-08x^3 - 9.152704E-06x^2 + 6.183222E-04x - 1.868122E-03$
α (P,2)	0
α (P,3)	$1.052982E-06x^3 - 2.300275E-04x^2 + 1.746666E-02x - 1.934927E-01$
α (P,4)	$-1.578387E-07x^3 + 3.514843E-05x^2 - 2.875965E-03x + 1.165695E-01$
α (P,5)	$-1.356629E-08x^3 + 2.907109E-06x^2 - 2.183847E-04x + 7.182448E-03$
α (P,6)	$1.351008E-07x^3 - 2.997332E-05x^2 + 2.331314E-03x - 2.433437E-02$
α (MA,1)	$1.092181E-09x^3 - 2.703439E-07x^2 + 3.001536E-05x - 5.907500E-04$
α (MA,2)	0
α (MA,3)	0
α (MA,4)	0
α (MA,5)	0
α (MA,6)	0

^ax is the ratio of VOC to NO_x (VOC/NO_x, ppbC/ppb)

^bIn α (j, i), j denotes heterogeneous reactivity (fast (F), medium (M), slow (S), partitioning only (P), multi-alcohol (MA)) and i denotes volatility (vapor pressure) (10^{-8} (1), 10^{-6} (2), 10^{-5} (3), 10^{-4} (4), 10^{-3} (5), 10^{-2} (6)) (mmHg) of lumping structure.

Figure S9. Model simulation for toluene SOA yields and oligomer fractions of the total organic matter (OM_{AR}/OM_T) under various VOC/ NO_x conditions.



The simulations employ the environmental condition of the experiment performed on 01/06/12 with 30ppb of toluene. The total OM yields were higher in lower NO_x conditions and lower in higher NO_x conditions, which is consistent with the results of other laboratory studies. The oligomer fraction (OM_{AR}/OM_T , black line) to the total OM shows different pattern. The model shows that oligomer fraction was highest at VOC/ NO_x ratio is near 10 and decrease either as NO_x increases or decreases.

References

- Barton, A. F. M.: CRC Handbook of Solubility Parameters and Other Cohesion Parameters, 2nd ed., CRC Press. Inc., Boca Raton, 1991.
- Bretti, C., Crea, F., Foti, C., and Sammartano, S.: Solubility and Activity Coefficients of Acidic and Basic Nonelectrolytes in Aqueous Salt Solutions. 1. Solubility and Activity Coefficients of o-Phthalic Acid and L-Cystine in NaCl (aq), (CH₃)₄NCl (aq), and (C₂H₅)₄NI (aq) at Different Ionic Strengths and at t = 25 C, *J. Chem. Eng. Data*, 50, 1761–1767, 2005.
- Cao, G., and Jang, M.: An SOA Model for Toluene Oxidation in the presence of Inorganic Aerosols, *Environ. Sci. Technol.*, 44, 727-733, 2010.
- Febo, A., and Perrino, C.: Prediction and Experimental Evidence for High Air Concentration of Nitrous Acid in Indoor Environments, *Atmos. Environ.*, 25A, 1055–1061, 1991.
- Jang, M., and Kamens, R. M.: Atmospheric Secondary Aerosol Formation by Heterogeneous Reactions of Aldehydes in the Presence of a Sulfuric Acid Aerosol Catalyst *Environ. Sci. Technol.*, 35, 4758–4766, 2001.
- Jang, M., Cao, G., and P., J.: Acidity Measurement of Atmospheric Aerosol by a Colorimetric Analysis, *Aerosol Science and Technology*, 42, 409-420, 2008.
- Keyword, M. D., Varutbangkul, V., Bahreini, R., Flagan, R. C., and Seinfeld, J. H.: Secondary organic aerosol formation from the ozonolysis of cycloalkenes and related compounds, *Environ. Sci. Technol.*, 38, 4157–4164, 2004.
- Li, J., and Jang, M.: Aerosol Acidity Measurement Using Colorimetry Coupled With a Reflectance UV-Visible Spectrometer *Aerosol Sci. and Technol.*, 46, 833–842, 2012.
- Liggio, J., and Li, S. M.: Organosulfate formation during the uptake of pinonaldehyde on acidic sulfate aerosols, *Geophys. Res. Lett.*, 33, L13808, 2006.
- Noubigh, A., Mgaidi, A., Abderrabba, M., Provost, E., and Furst, W.: Effect of salts on the solubility of phenolic compounds: experimental measurements and modelling, *J. Sci. Food Agric.*, 87, 783–788, 2007.
- Pankow, J.: absorption model of gas/particle partitioning of organic compounds in the atmosphere, *Atmos. Environ.*, 28, 185–188, 1994.
- Segatin, N., and Klofutar, C.: Salting-out of some alkyl acetates in aqueous sodium chloride solutions, *Monatsh. Chem.*, 131, 131–144, 2000.